Synthesis and use of new porous metal complexes containing a fusidate moiety as gas storage media

Zinah Nazih Mahmood*, Mahasin Alias*, Gamal Abdel-Rahman El-Hiti,†,
Dina Saadi Ahmed***, and Emad Yousif******

*Department of Chemistry, College of Science for Women, University of Baghdad, Baghdad, Iraq
**Cornea Research Chair, Department of Optometry, College of Applied Medical Sciences, King Saud University,
P.O. Box 10219, Riyadh 11433, Saudi Arabia
***Department of Medical Instrumentation Engineering, Al-Mansour University College, Baghdad 64021, Iraq
****Department of Chemistry, College of Science, Al-Nahrain University, Baghdad 64021, Iraq
(*Received 2 August 2020 • Revised 17 September 2020 • Accepted 3 October 2020*)

Abstract−The burning of fossil fuels produces carbon dioxide emissions, increased levels of which cause serious environmental problems. Therefore, the design and use of new materials as media for capturing carbon dioxide and other gases, such as hydrogen and methane, has attracted significant research attention. In this work, three metal complexes containing a fusidate moiety were synthesized and tested as storage media for gases. By reacting sodium fusidate and metal chlorides in boiling ethanol, the corresponding metal complexes were obtained with 69-76% yields. The fusidate moiety acts as a bidentate ligand with variable geometry (distortion octahedral, square planner, or tetrahedral) depending on the metal (manganese, copper, or zinc, respectively) it is associated with. The elemental composition of the metal complexes was confirmed via energy dispersive X-ray spectroscopy and their surface morphology was inspected via field emission scanning electron microscopy. The Brunauer-Emmett-Teller surface area of the metal complexes varied from 31.2 to 46.9 m^2/g, with pore volume and diameters of 0.035-0.049 cm^3/g and 3.02-3.18 nm, respectively. The gas uptake at 323 K for carbon dioxide, hydrogen, and methane depended on the metal, gas, surface pore volume, and pore diameter. Reasonable carbon dioxide uptake (6.3-7.2 wt%) was achieved with fusidate metal complexes at high temperature and pressure, whereas hydrogen and methane slowly permeated throughout the complexes.

Keywords: Fusidate Metal Complexes, Gas Storage Media, Environmental Pollution, Carbon Dioxide Uptake, Surface Area, Adsorption

INTRODUCTION

Over time, the consumption of natural gas and oil has increased with rising energy demands, raising carbon emissions to unacceptable levels. High concentrations of carbon dioxide (CO_2) in the air are linked to several serious problems [1], particularly global warming and its associated climate changes, pollution, and worldwide natural disasters [2]. Therefore, several strategies have been developed to generate energy while mitigating the problems associated with high carbon emissions. Renewable sources of energy such as solar, biomass, and wind are low-carbon and environmentally friendly [3,4]. In principle, the exclusive use of these sources could cut CO_2 emissions to zero [5,6]. The energy produced from these renewable sources has many advantages compared to that produced from fossil fuels. However, it suffers from high startup or installation cost, intermittent availability throughout the year, geographic constraints, and limited long-term storage capacity [7]. In addition, these sources are not yet capable of providing enough energy to meet global needs. Although nuclear energy could fulfill the global requirement for clean, reliable, and cost-effective electricity, post-fission waste,

the high cost of its disposal, and the possibility of leaks or other catastrophic accidents hinders its use [8].

Another strategy to reduce environmental CO_2 levels is to capture and store it [9-12]. However, the development of efficient and reliable materials as storage media for CO_2 has been a persistent challenge [13,14]. The emitted CO_2 is captured via physical or chemical adsorption over a certain absorber. These two most common adsorption approaches are both highly dependent on the interaction between adsorbent and gas. Physical adsorption involves trapping of the gas within the pores of a porous material, whereas chemical adsorption involves the formation of hydrogen bonds between the gas and the adsorbent. Chemical adsorption using ammonia or ethanolamine has had limited success given the high operating costs and energy inputs required [15,16]. These problems persist across amines as a class of sorbents because they are expensive, prone to degradation in the presence of oxygen or sulfur dioxide and are volatile. Research has made some progress in reducing the cost and temperature required for amine-based systems, but such systems remain only partially effective [17,18]. Thus, other materials have been designed and synthesized to be used as effective CO_2 capturing media.

Activated carbons, silica, zeolites, covalent organic frameworks, conjugated microporous polymers, and cross-linked polymers have all been studied as adsorbents for CO_2 [19]. The pore size and ad-

sorption capacity of these porous materials determines their efficiency as gas storage media [20,21]. Limited success has been achieved using highly hydrophilic materials (e.g., silica, and zeolites); in contrast, activated carbons have demonstrated poor gas selectivity and require the use of an activator [22-24]. Greater success has been achieved using metal organic frameworks (MOFs) and porous organic polymers (POPs) as gas storage media owing to their high surface areas [25,26]. However, the synthetic pathways for these materials require extreme conditions and precious metal-based catalysts, rendering them expensive and challenging to synthesize [27].

Recently, we synthesized several porous materials and explored their potential use in capturing CO_2 [28-32]. In this work, we report the synthesis of three new metal complexes containing a fusidate moiety and their use as storage media for carbon dioxide, methane (CH_4), and hydrogen (H_2). Our precursor, sodium fusidate, is stable, non-toxic [33], commercially available, has a high molecular weight with a high oxygen content (*ca.* 18%), and possesses different oxygen-containing functional groups (ester, and hydroxy moieties). These properties enable the fusidate metal complexes to exhibit similar behavior to MOFs and POPs as gas storage media.

EXPERIMENTAL

1. General

Sodium fusidate (99.5%), metal chlorides (analytical grade), and solvents were purchased from Merck (Schnelldorf, Germany). A Vario EL III elemental analyzer (Elementar Analysensysteme GmbH; Langenselbold, Germany) was used to determine the elemental composition of the complexes. The metal content was determined using an AA-6880 Shimadzu atomic absorption flame spectrophotometer (Shimadzu Corporation; Tokyo, Japan). The Fourier transform infrared (FTIR) spectra were recorded on an FT-IR 8300 Shimadzu spectrophotometer (Shimadzu Corporation; Tokyo, Japan). The ultraviolet-visible (UV-Vis) spectra were measured in dimethyl sulfoxide (DMSO) using a Shimadzu UV-1601 spectrophotometer (Shimadzu Corporation; Tokyo, Japan). The conductivity was measured on a ProfiLine Oxi 3205 instrument (Xylem Analytics; Weinheim, Germany). The energy dispersive X-ray (EDX) and field emission scanning electron microscopy (FESEM) images were recorded using a Tescan MIRA3 LMU instrument (Tescan Orsay Holding; Brno-Kohoutovice, Czech Republic).

2. Synthesis of Metal Complexes

A mixture of sodium fusidate (1.08 g, 2.0 mmol) and appropriate metal chloride (1.0 mmol) in ethanol (EtOH; 10 mL) was refluxed for 3 h. The solid formed was collected via filtration, washed with water (3×10 mL), dried, and recrystallized from EtOH to give the corresponding metal complex.

3. Nitrogen Gas Adsorption Measurements

A vacuum oven was used to dry the samples for 4 h at 60 °C prior to the measurements. The Brunauer-Emmett-Teller (BET) method was used to measure the specific surface area from the nitrogen (N_2) adsorption isotherms. Pore size and pore volume were measured via the Barrett-Joyner-Halenda (BJH) method [34].

4. Gas Storage Measurements

The gas uptake of the complexes was determined using an H-sorb 2600 high-pressure volumetric adsorption instrument. The complexes (1 g) were degassed in a vacuum oven (50 °C) for 1 h to remove any water or solvent trapped within the pores. The gas uptake experiment was then replicated several times under identical conditions for each complex to determine the optimum pressure. The adsorption experiments system includes the use of a gas compressor and a gas cylinder that are connected via a pipe based on previous reports [35,36]. The detailed method and apparatus diagram for gas uptake experiments have been previously reported [35,36].

RESULTS AND DISCUSSION

1. Synthesis and Characterization of Metal Complexes

The reaction of sodium fusidate (two molar equivalents) and manganese chloride tetrahydrate ($MnCl_2 \cdot 4H_2O$) in refluxing ethanol for 2 h produced the corresponding hydrated Mn complex (Scheme 1) with 71% yield. Similarly, the reaction of sodium fusidate and copper or zinc chloride ($CuCl_2$ or $ZnCl_2$) produced the corresponding metal complex (Scheme 2) in 76% or 69% yields, respectively. Table 1 lists the elemental compositions and some physi-
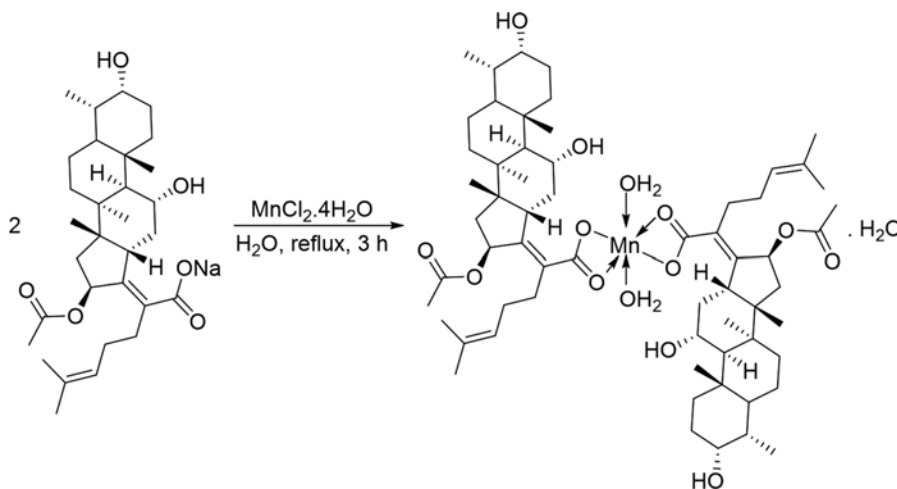
Scheme 1. Synthesis of the Mn(II) complex.
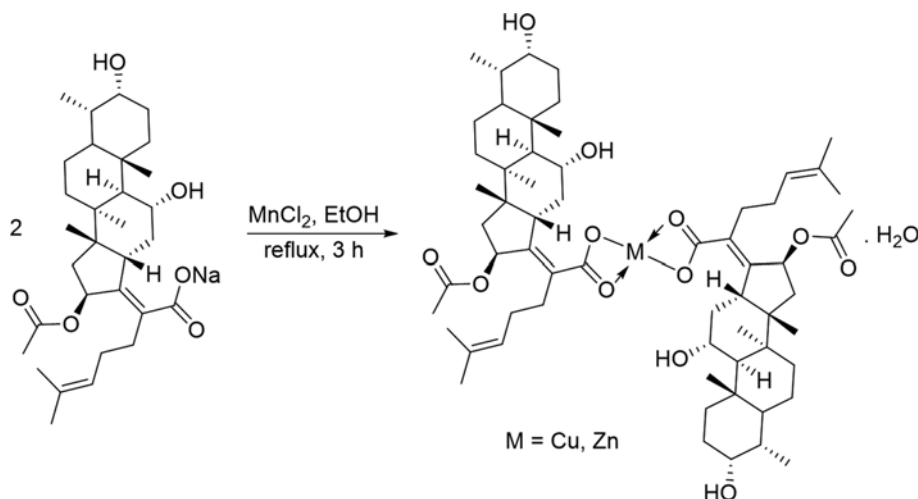
Scheme 2. Synthesis of the Cu (II) and Zn(II) complexes.

Table 1. Color, melting point, yield, and elemental composition of fusidate metal complexes

Complex	Color	Melting point (°C)	Yield (%)	Calculated (Found; %)		
				C	H	M
Mn(II)	Light pink	172-174	71	65.30 (65.64)	8.84 (8.96)	4.82 (4.86)
Cu(II)	Green	178-180	76	66.91 (67.28)	8.69 (8.71)	5.71 (5.75)
Zn(II)	Off-white	160-162	69	66.80 (66.82)	8.68 (8.70)	5.86 (5.87)

Table 2. Selected FTIR absorption bands of fusidate metal complexes

Complex	νOH	νCOO (ester)	νCOO (asym)	νCOO (sym)	νC-OH	νM-O
Mn(II)	3,410	1,708	1,530	1,377	1,269	516
Cu(II)	3,495, 3,441	1,712	1,520	1,381	1,265	451
Zn(II)	3,483, 3,460	1,712	1,523	1,377	1,265	424

Table 3. Electronic transitions, conductivity, and suggested geometry of metal complexes

Complex	Absorption (cm^{-1})	Assignments	Conductivity (µS/cm)	Suggested geometry
Mn(II)	11,111 20,920	$^6A_1g \rightarrow {}^4T_1g_{(G)}$ $^6A_1g \rightarrow {}^4T_2g_{(G)}$	11.4	Distorted octahedral
Cu(II)	14,492 35,087	$^2B_1g \rightarrow {}^2A_1g, {}^2B_2g, {}^2Eg$ L$\rightarrow$CuCT	10.9	Square planner
Zn(II)	35,842 40,485 43,478	ILCT	9.9	Tetrahedral

cal properties of the fusidate metal complexes.

Energy dispersive X-ray spectroscopy (EDX) was used to determine the elemental composition of the fusidate metal complexes [37]. The EDX graphs (Fig. S1-S3) show the presence of both metals and the other elements contained in the fusidate moiety.

The FTIR spectra of the metal complexes (Fig. S4-S6) were recorded and analyzed (Table 2) to determine the nature of the functional groups within the complexes [38-40]. The FTIR spectra show broad absorption bands within the 3,410-3,495 cm^{-1} region that correspond to hydroxyl groups, and the carbonyl of the ester group

(O-C=O) shows strong absorption bands at 1,708-1,712 cm^{-1}. The absorption bands corresponding to the asymmetric (ν_{asym}) and symmetric (ν_{sym}) vibrations of the C=O of the ester group appeared between 1,520-1,530 and 1,377-1,381 cm^{-1}, respectively (Table 2). The difference between the ν_{asym} and ν_{sym} ($\Delta\nu$) for the C=O of the ester group for all complexes ranged from 139 to 153 cm^{-1}, indicating bidentate bridging [41]. New absorption bands from the formation of Mn-O, Cu-O, and Zn-O bonds were observed at 516, 451, and 424 cm^{-1}, respectively. The broad bands around 3,610-3,224 cm^{-1} are attributed to water molecules within the complexes, similar

to the bands observed at 921, 860, and 848 cm^{-1}, which are associated with the rocking and wagging of water within the Mn, Cu, and Zn complexes. The wavenumbers of these bands indicate that water is present within the field of coordination [42]. Generally, the variation in wavenumber for the complexes was minimal.

The UV-Vis spectra of the metal fusidate complexes are shown in Fig. S7-S9. The Mn complex exhibits bands at 11,111 and 20,920 cm^{-1}, which are assigned to $^6A_1g{\rightarrow}^4T_1g_{(G)}$ and $^6A_1g{\rightarrow}^4T_2g_{(G)}$ transitions, respectively (Table 3) [43]. For the Cu complex, the UV-Vis spectrum exhibits a broad absorption band at 14,492 cm^{-1} owing
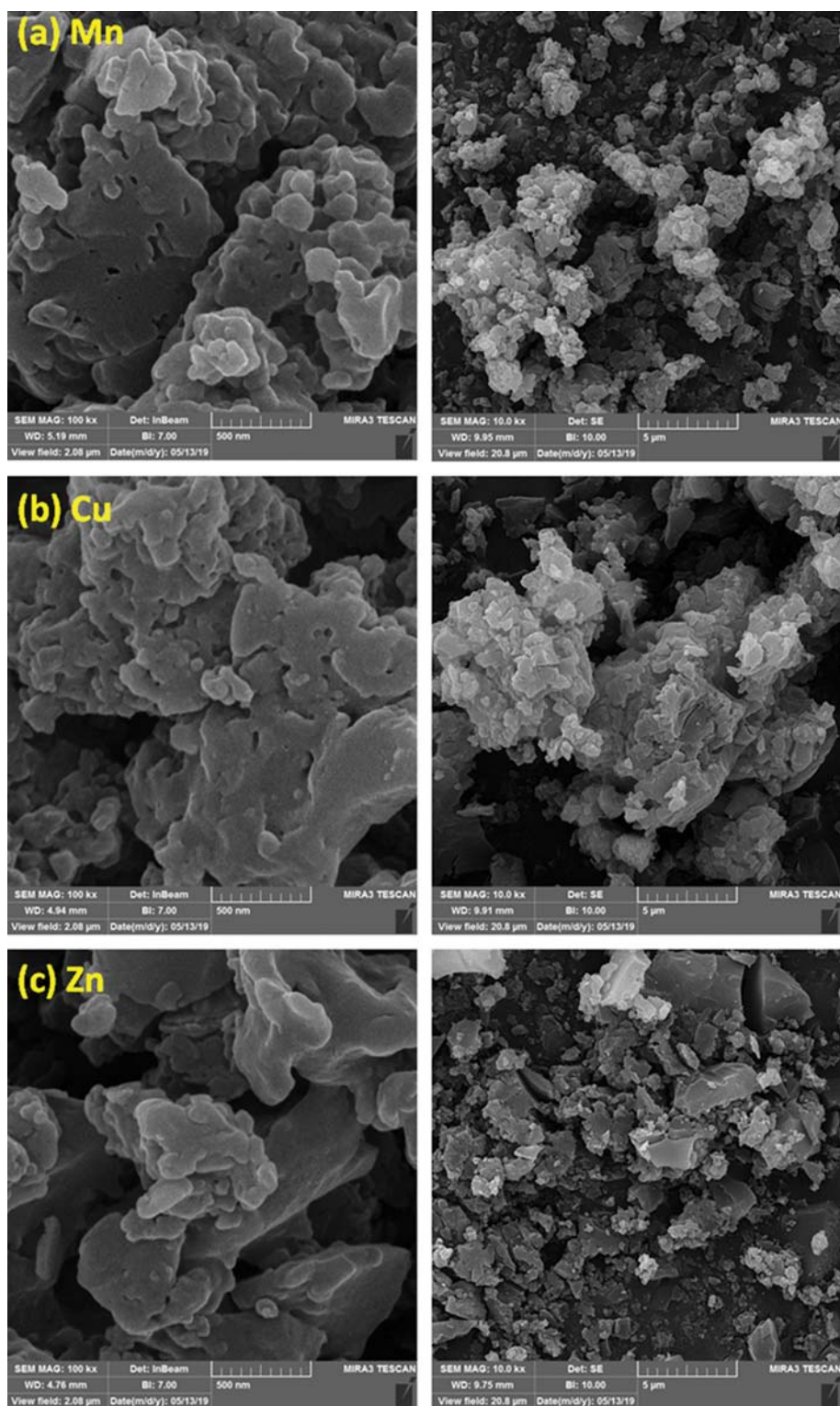

Fig. 1. Field emission scanning electron microscopy images of (a) Mn(II), (b) Cu(II), and (c) Zn(II) complexes.

to the $^2B_1g \rightarrow ^2A_1g$, ^2B_2g, and ^2Eg transitions. Additionally, it exhibits a band at 35,087 cm^{-1}, corresponding to the charge transfer (CT) states observed in the electronic spectrum [44]. The Zn complex is diamagnetic, with no d-d transitions (d^{10}); however, the positions of the bands do shift upon complexation with zinc when compared to that of sodium fusidate (i.e., free ligand) [45]. The absorption bands at 35,842, 40,485, and 43,478 cm^{-1} are attributed to intra-ligand charge transfer (ILCT) [46]. The suggested geometries for the Mn, Cu, and Zn complexes are distorted octahedral, square planar, and tetrahedral, respectively. The conductivity of the metal complexes varied from 9.9 to 114 µS/cm and indicated nonionic behavior [47].

2. Surface Morphology of Metal Complexes

The surface morphology of the fusidate metal complexes was inspected via FESEM. Fig. 1 shows that the fusidate metal complexes have heterogeneous and porous structures. In addition, the FESEM images show tiny particle agglomerates of various shapes and sizes. The particle sizes were found to range between 28.6-43.3, 36.8-48.8, and 39.7-49.7 nm for the Mn, Cu, and Zn complexes, respectively.

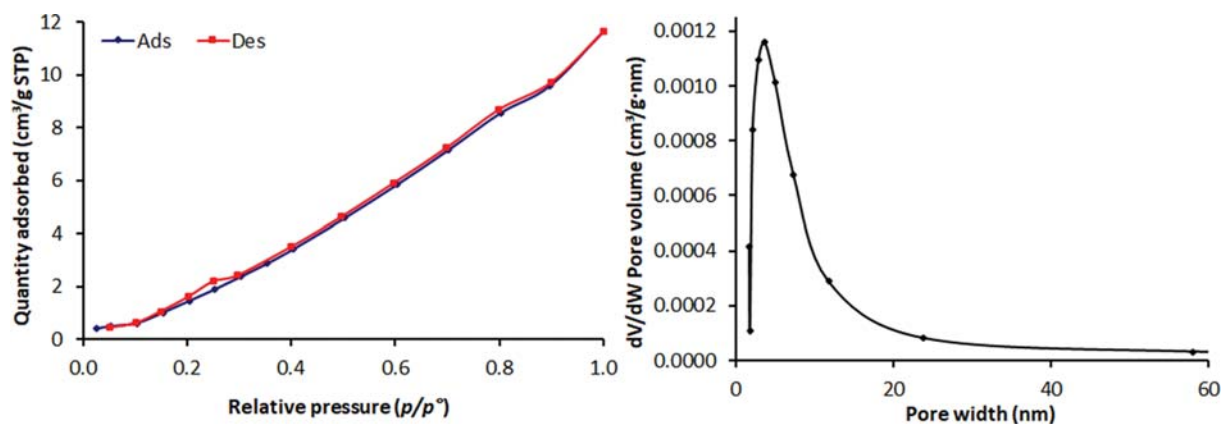

Fig. 2. N$_2$ adsorbed isotherms and pore size distribution of Mn(II) complex.
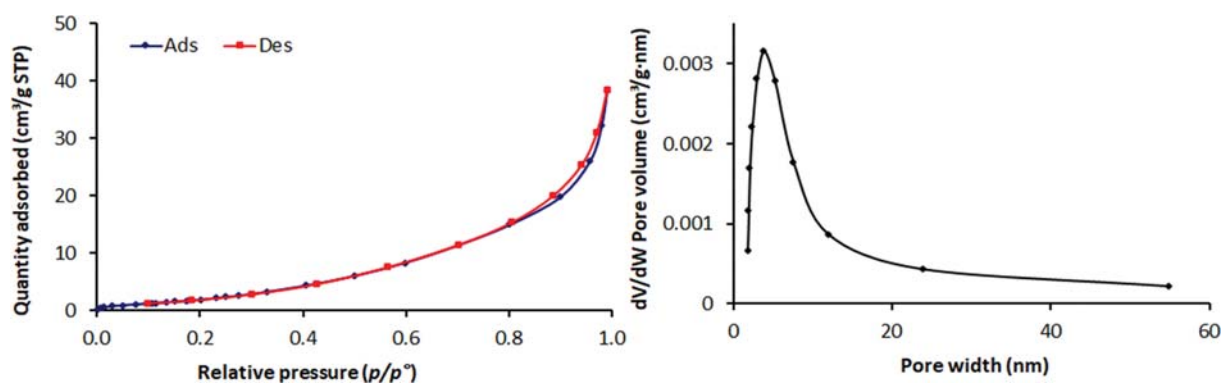

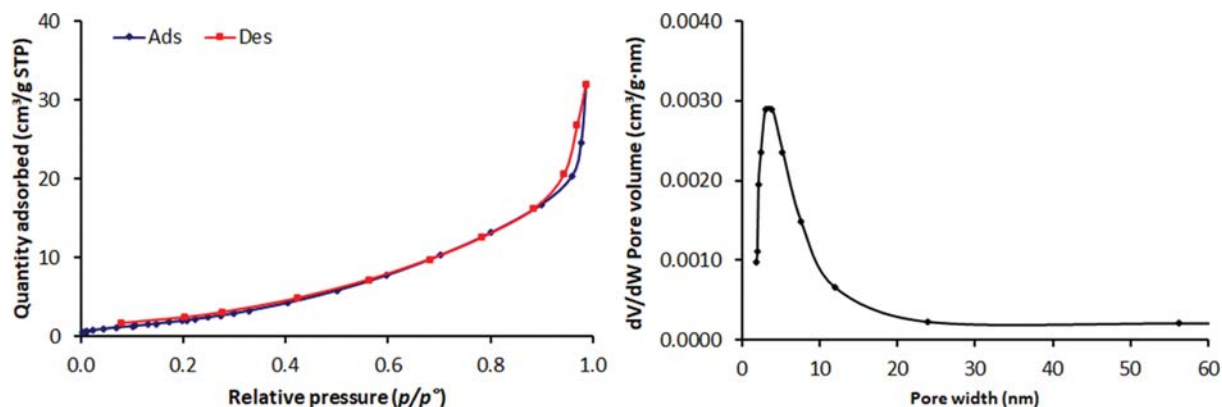Fig. 3. N$_2$ adsorbed isotherms and pore size distribution of Cu(II) complex.

Fig. 4. N$_2$ adsorbed isotherms and pore size distribution of Zn(II) complex.

Table 4. Surface area and pore size distributions of metal complexes obtained via N_2 adsorption

Complex	S_{BET} (m^2/g)	Pore volume (cm^3/g)	Average pore diameter (nm)
Mn(II)	46.9	0.049	3.18
Cu(II)	35.5	0.039	3.05
Zn(II)	31.2	0.035	3.02

3. BET Surface Area Determination of Metal Complexes

The adsorption capacity of adsorbent materials is commonly determined using their BET surface area, making it critical that the gas adsorption capacity of porous materials is measured from their nitrogen isotherms [48]. The porosity of adsorbents provides valuable information on their physical and chemical interactions with adsorbed gas. Therefore, the nitrogen isotherms and pore size distributions of the fusidate metal complexes were determined (Fig. 2-4) using the nitrogen adsorption-desorption graphs overlaid for all metal complexes. Based on the isotherms, the interactions between adsorbent and adsorbate were deemed relatively weak as the metal complexes have type IV mesoporous structures with no identifiable monolayer formation [49,50]. The hysteresis loops observed are typical for H3 type mesoporous materials with the H3: hysteresis loop allied with slit-shaped pores. The BET surface area and pore volumes were calculated from the nitrogen adsorption isotherms at $P/P^o=0.9$ and the average pore diameters were calculated from the desorption data using the BJH method (Table 4). The BET surface areas of the fusidate metal complexes were 31.2-46.9 m^2/g. The pore volumes and diameters were 0.035-0.049 cm^3/g and 3.02-3.18 nm. The Mn complex was found to have the highest BET surface area, pore volume, and pore diameter.

4. Gas Uptake of Metal Complexes

Gas adsorption is highly dependent on the pore size, charge of the metal and ligand, and strength of the interaction between the adsorbent and adsorbate (e.g., van der Waal forces or hydrogen bonds) [51]. High energy input is required for the gas to be adsorbed if the aperture size is small when compared to the molecular size of the adsorbate and can allow repulsive forces to dominate [51]. The pore volumes play a vital role in determining the gas uptake capacity of adsorbent materials as materials with large pore volumes can store more gases [52,53]. Several conditions were attempted in which the pressure was varied from 1 to 50 bars for optimization. The complexes showed the highest CO_2 uptake at 50 bars. The CO_2, CH_4, and H_2 uptake by the fusidate metal complexes was recorded at 323 K and 50 bars of the adsorbate of interest and is summarized in Table 5. The gas adsorption isotherms for metal complexes are shown in Fig. 5-7.

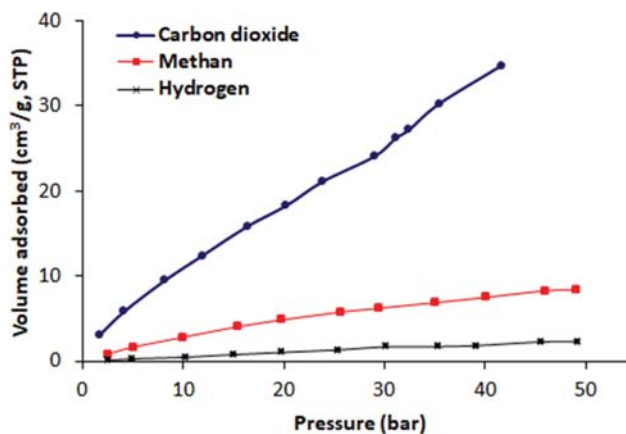The CO_2 uptake capacity of the fusidate metal complexes is

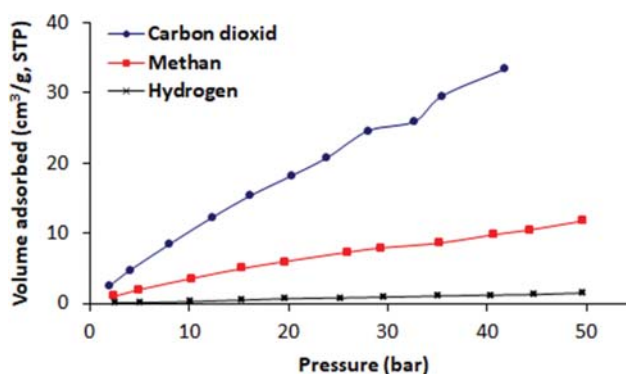Fig. 5. Gas adsorption isotherms for Mn(II) complex.

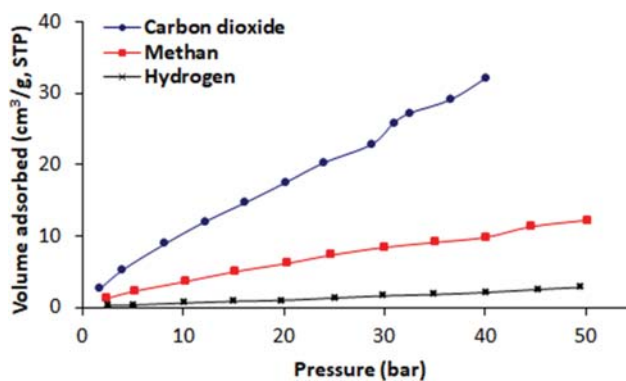Fig. 6. Gas adsorption isotherms for Cu(II) complex.

Fig. 7. Gas adsorption isotherms for Zn(II) complex.

higher than that determined for CH_4 and H_2. Such variations could be due to the differences between the polarizability of CO_2, CH_4,

Table 5. Metal complexes gas uptakes of CO_2, H_2, and CH_4 at 323 K and 50 bar

Complex	CO_2 (cm^3/g)	CO_2 (wt%)	H_2 (cm^3/g)	H_2 (wt%)	CH_4 (cm^3/g)	CH_4 (wt%)
Mn(II)	34.8	7.2	2.3	0.023	8.4	0.631
Cu(II)	33.4	6.7	1.5	0.014	11.8	0.841
Zn(II)	32.2	6.3	2.8	0.026	12.2	0.887

and H_2. For example, CO_2 has a strong quadrupole moment, which leads to a high adsorption capacity as it is more diffusible [54]. The strong attractive forces, such as van der Waals forces or electrostatic forces (e.g., surface field-molecular dipole interactions and polarization force), between the metal complexes and CO_2 could also lead to higher gas uptake [25]. Generally, the adsorption process occurs through a combination of different interactions. CH_4 and H_2 are non-polar with weak attractions to the surface of the metal complexes, which could lead to their low adsorption capacity [54].

The Mn complex has the highest BET surface area and pore diameter of the samples studied. Notably, the Mn complex had the highest gas uptake (Fig. 5) when compared to the Cu (Fig. 6) and Zn (Fig. 7) complexes. The Mn complex has a significant CO_2 uptake of 7.2 wt% compared to the 6.3 and 6.7 wt% of the Cu and Zn complexes, respectively. This could be due to the water molecules attached to the Mn metal centers in the framework that enhance the pores-surfaces for adsorption [55]. The functional groups within the fusidate unit might enhance the physical attractions with gas molecules.

H_2 diffusion through the metal complexes was expected to be higher than that observed for CO_2 and CH_4 as H_2 has a smaller molecular size. However, high accumulative H_2 adsorption on the surface of other metal complexes blocked the pores and prevented diffusion [56]. Clearly, the more strongly condensable gas being preferentially adsorbed within the pores of the metal complex reduces the open porosity. The metal complexes used herein are more suitable for storing more strongly absorbable gases (CH_4 and CO_2) rather than non-condensable or weakly absorbable gases (H_2) [57]. The lack of binding sites with high affinity between the metal complexes and hydrogen is likely the main reason for its low storage capacity. The manipulation of pore volumes, pore diameters, and surface areas of the adsorbents is a possible route for improving the H_2 storage capacity and adsorption enthalpy of such systems [58].

The use of porous nanocarbons/base system led to CO_2 capture as 1.9 to 4.6 mmol/g (25 °C) [24]. While, the capture of CO_2 over polyacrylonitrile/potassium hydroxide and resorcinol/formaldehyde/ potassium hydroxide systems (25 °C and 1 bar) was 2.74 and 4.95 mmol/g, respectively [22,59]. Similarly, zeolite 13X was used as media for CO_2 storage and the gas uptake was 4.22 mmol/g (25 °C and 1 bar) [36]. Melamine Schiff bases [31] and polyphosphate containing benzidine [32] showed high CO_2 uptake at 10 and 14 wt%, respectively, due to their high surface area and aromaticity content In this work, the CO_2 uptake (up to 7.3 wt%) over fusidate-metal complexes was higher than those reported over polyphosphates containing 1,4-diaminobenzene (6.0 wt%) [28], valsartan-metal complexes (6.8 wt%) [29], and telmisartan-tin complexes (7.1 wt%) [30].

CONCLUSIONS

Herein, three metal complexes containing a fusidate moiety were synthesized and their chemical structures were established. The metal complexes have particles that vary in shape, size, and diameter. The manganese complex had the highest surface area (46.9 m^2/g) when compared to copper (35.5 m^2/g) and zinc (31.2 m^2/g) complexes. Similarly, the pore volume and diameter were higher for the man-

ganese complex compared to the other two complexes. The gas uptake depended on the type of gas, metal, and the surface pore volume and diameter. The complexes used were inefficient hydrogen and methane adsorbents, as these gases slowly permeate throughout the complexes The manganese complex was the most efficient as a CO_2 storage medium (7.2 wt%).

ACKNOWLEDGEMENTS

SUPPORTING INFORMATION

Additional information as noted in the text. This information is available via the Internet at http://www.springer.com/chemistry/ journal/11814.

REFERENCES

1. K. L. Lim, H. Kazemian, Z. Yaakob and W. R. W. Daud. *Chem. Eng. Technol.*, **33**, 213 (2010).
2. P. A. Owusu and S. Asumadu-Sarkodie, *Cogent. Eng.*, **3**, 1167990 (2016).
3. A. Qazi, F. Hussain, N. A. Rahim, G. Hardaker, D. Alghazzawi, K. Shaban and K. Haruna, *IEEE Access*, **7**, 63837 (2019).
4. N. A. Ludin, N. I. Mustafa, M. M. Hanafiah, M. A. Ibrahim, M. A. M. Teridi, S. Sepeai, A. Zaharim and K Sopian, *Renew. Sustain. Energy Rev.*, **96**, 11 (2018).
5. F. Fornara, P. Pattitoni, M. Mura and E. Strazzera, *J. Environ. Psychol.*, **45**, 1 (2016).
6. A. Mardani, A. Jusoh, E. K. Zavadskas, E. Cavallaro and Z. Khalifah *Sustainability*, **7**, 13947 (2015).
7. A. Azarpour, S. Suhaimi, G. Zahedi and A. Bahador, *Arab. J. Sci. Eng.*, **38**, 317 (2013).
8. M. Ho, E. Obbard, P. A. Burr and G. Yeoh, *Energy Procedia*, **160**, 459 (2019).
9. F. C. Carvalho, P. F. Nascimento, M. R. O. Souza and A. S. Araujo, *Processes*, **8**, 289 (2020).
10. M. Busu, *Processes*, **7**, 923 (2019).
11. A. Borhan, S. Yusup, J. W. Lim and P. L. Show, *Processes*, **7**, 855 (2019).
12. M. Razavian, S. Fatemi and M. Masoudi-Nejad, *Adsorpt. Sci. Technol.*, **32**, 73 (2014).
13. H. Li, L. Li, R.-B. Lin, W. Zhou, Z. Zhang, S. Xiang and B. Chen, *EnergyChem*, **1**, 100006 (2019).
14. H. Lyu, Q. Zhang, Y. Wang and J. Duan, *Dalton Trans.*, **47**, 4424 (2018).
15. D. Y. C. Leung, G. Caramanna and M. M. Maroto-Valer, *Renew. Sustain. Energy Rev.*, **39**, 426 (2014).
16. L. Raynal, P.-A. Bouillon, A. Gomez and P. Broutin. *Chem. Eng. J.*, **171**, 742 (2011).
17. E. J. Novek, E. Shaulsky, Z. S. Fishman, L. D. Pfefferle and M. Elimelech, *Environ. Sci. Technol. Lett.*, **3**, 291 (2016).

18. Q. Zhuang, R. Pomalis, L. Zheng and B. Clements, *Energy Procedia*, **4**, 1459 (2011).

19. C. Lu, T. Ben and S. Qiu, *Macromol. Chem. Phys.*, **217**, 1995 (2016).

20. T. Liu, J. Ding, Z. Su and G. Wei, *Mater. Today Energy*, **6**, 79 (2017).

21. Q.-R. Fang, T. A. Makal, M. D. Young and H.-C. Zhou, *Comment Inorg. Chem.*, **31**, 165 (2010).

22. Y.-C. Chiang, C. Y. Yeh and C. H. Weng, *Appl. Sci.*, **9**, 1977 (2019).

23. E. H. Al-Ghurabi, A. Ajbar and M. Asif, *Appl. Sci.*, **8**, 1467 (2018).

24. P. Staciwa, U. Narkiewicz, D. Moszyński, R. J. Wróbel and R. D. Cormia, *Appl. Sci.*, **9**, 3349 (2019).

25. D. S. Ahmed, G. A. El-Hiti, E. Yousif, A. A. Ali and A. S. Hameed, *J. Polym. Res.*, **25**, 75 (2018).

26. R. Dawson, A. I. Cooper and D. J. Adams, *Prog. Polym. Sci.*, **37**, 530 (2012).

27. W. Wang, M. Zhou and D. Yuan, *J. Mater. Chem. A*, **5**, 1334 (2017).

28. H. A. Satar, A. A. Ahmed, E. Yousif, D. S. Ahmed, M. F. Alotibi and G. A. El-Hiti, *Appl. Sci.*, **9**, 4314 (2019).

29. A. Mohammed, E. Yousif and G. A. El-Hiti, *Materials*, **13**, 1183 (2020).

30. A. G. Hadi, K. Jawad, E. Yousif, G. A. El-Hiti, M. H. Alotaibi and D. S. Ahmed, *Molecules*, **24**, 1631 (2019).

31. R. M. Omer, E. T. B. Al-Tikrity, G. A. El-Hiti, M. F. Alotibi, D. S. Ahmed and E. Yousif, *Processes*, **8**, 17 (2020).

32. D. S. Ahmed, G. A. El-Hiti, E. Yousif, A. S. Hameed and M. Abdalla, *Polymers*, **9**, 336 (2017).

33. M. E. Falagas, A. P. Grammatikos and A. Michalopoulos, *Expert. Rev. Anti. Infect. Ther.*, **6**, 593 (2008).

34. K. Sing, *Colloids Surf.*, **187-188**, 3 (2001).

35. M. Pellerano, P. Pre, M. Kacem and A. Delebarre, *Energy Procedia*, **1**, 647 (2009).

36. L. Hauchhum and P. Mahanta, *Int. J. Energy Environ. Eng.*, **5**, 349 (2014).

37. R. Gangadhar, K. A. Jaleeli and A. Ahmad, *Int. J. Sci. Environ. Technol.*, **4**, 1195 (2015).

38. Y. R. Sharma, *Elementary organic spectroscopy: Principles and chemical applications*, S Chad & Company Ltd, New Delhi, India (2008).

39. M. Ibrahim, A. Nada and D. E. Kamal, *Indian J. Pure Appl. Phys.*, **43**, 911 (2005).

40. A. A. Awad, M. M. Hasson, A. A. Fadhel and B. F. Alfarhani, *J. Phys. Conf. Series*, **1294**, 052040 (2019).

41. Q.-Q. Xiao, D. Liu, Y.-L. Wei and G.-H. Cui, *J. Solid State Chem.*, **273**, 67 (2019).

42. G. B. Deacon and R. J. Phillips, *Coordin. Chem. Rev.*, **33**, 227 (1980).

43. M. Alias, H. Kassum and C. Shakir, *J. King Saud Uni. Sci.*, **25**, 157 (2013).

44. M. F. Alias and A. S. Basha'ar, *Baghdad Sci. J.*, **11**, 1556 (2014).

45. M. F. Alias and A. N. Seewan, *Diyala J. Pure Sci.*, **9**, 93 (2013).

46. H. E. L. Hamdani and M. E. L. Amane, *J. Mol. Struct.*, **1184**, 262 (2019).

47. N. I. Dodoffa, D. Kovala-Demertzi, M. Kubiak, J. Kuduk-Jaworska, A. Kochel and G. A. Gorneva, *Z. Naturforsch. B Chem. Sci.*, **61**, 1110 (2006).

48. B. R. Vergis, N. Kottam, R. H. Krishna and B. M. Nagabhushana, *Nano-Struct. Nano-Objects*, **18**, 100290 (2019).

49. M. Thommes, K. Kaneko, A. V. Neimark, J. P. Olivier, F. Rodriguez-Reinoso, J. Rouquerol and K. S. W. Sing, *Pure Appl. Chem.*, **87**, 1051 (2015).

50. K. A. Cychosz and M. Thommes, *Engineering*, **4**, 559 (2018).

51. A. Khadilkar and S. Chavan. *Bom. Technol.*, **59**, 44 (2009).

52. H. Furukawa and O. M. Yaghi, *J. Am. Chem. Soc.*, **131**, 8875 (2009).

43. Y. Peng, V. Krungleviciute, I. Eryazici, J. T. Hupp, O. K. Farha and T. Yildirim, *J. Am. Chem. Soc.*, **135**, 11887 (2013).

54. M. Razavian, S. Fatemi and M. Masoudi-Nejad, *Adsorpt. Sci. Technol.*, **32**, 73 (2014).

55. J.-R. Li, Y. Ma, M. C. McCarthy, J. Sculley, J. Yu, H.-K. Jeong, P. B. Balbuena and H.-C. Zhou, *Coord. Chem. Rev.*, **255**, 1791 (2011).

56. H. A. Ozen and B. Ozturk, *Sep. Purif. Technol.*, **211**, 514 (2019).

57. A. B. Fuertes, *J. Membr. Sci.*, **177**, 9 (2000).

58. Y. Xia, Z. Yang and Y. Zhu, *J. Mater. Chem. A*, **1**, 9365 (2013).

59. J. Choma, M. Kloske, A. Dziura, K. Stachurska and M. Jaroniec, *Eng. Prot. Environ.*, **19**, 169 (2016).